Polymer
Chemistry

PAPER

View Article Online
View Journal

Cite this: DOI: 10.1039/d5py00194c

Ion mobility mass spectrometry coupled with molecular dynamics simulations: in-depth structural analysis of polystyrene-based Au-containing copolymers†

Sarajit Naskar,[a,b,c] Aidan Izuagbe,[b] Vincent Lemaur,[c] Quentin Duez,[a] Andrea Minoia,[c] Julien De Winter,[a] Stephen J. Blanksby,[b] Jérôme Cornil,[c] Christopher Barner-Kowollik *[b,d] and Pascal Gerbaux *[a]

Received 26th February 2025,
Accepted 28th March 2025

DOI: 10.1039/d5py00194c

rsc.li/polymers

Artificial enzymes based on polystyrene copolymers featuring a metal complex within their structure, so-called single-chain nanoparticles (SCNPs), are being explored as hybrid heterogeneous/homogeneous catalysts. Using styrene (derivative) building blocks, SCNP precursor copolymers decorated with pendent triphenylphosphine ligands complexed with catalytically active gold motifs have recently been reported. It is highly challenging to determine the location and orientation of the functional groups – including the catalytic center – the coil geometry, and even the macromolecular architecture within these complex precursors *via* conventional analytical techniques. The use of ion mobility mass spectrometry (IMS-MS) combined with molecular dynamics (MD) simulations is emerging as a way to establish the structure of gaseous ions, including the description of the secondary interactions responsible for the folding. IMS-MS is used to separate intricate polymer mixtures, while providing structural information through collisional cross section (CCS) determination. MD simulations are used to assign a detailed internal structure to the conformations sampled by IMS-MS by comparing the experimental CCS with the theoretical values computed for the MD structures. In the present contribution, we provide an in-depth investigation of the conformation of gaseous Au-functionalized copolymer ions composed of three different monomer units, *i.e.*, styrene, styrene-CH_2-OH and styrene-PPh_2-AuCl, and those bearing a TEMPO unit as the initiator end group. For the styrene/styrene-CH_2-OH copolymer ions, an H-bond between protonated TEMPO and a styrene-CH_2-OH unit is responsible for the ultimate folding of the polymer ions with the charge settled at the center of the globular ions. When incorporating the triphenylphosphine-AuCl unit, a strong H-bond between the chlorine atom and protonated TEMPO is detected. However, the steric hindrance around the triphenylphosphine ligand prevents the charge from being incorporated into the core of the globular ions.

1. Introduction

Enzymes are known to catalyze biochemical reactions in aqueous environments in specific temperature and pH ranges, making them highly effective catalysts.[1] They are increasingly regarded as sources of inspiration for the development of a variety of synthetic enzyme-mimic catalysts based on polymers,[2,3] macromolecules,[4] and dendrimers.[5] Enzymes feature exceptional specificity[6] and catalytic activity[7] due to their unique structures, and transferring such properties to robust and cost-effective synthetic macromolecules is a rewarding strategy.[8–10]

Designing single-chain nanoparticles (SCNPs) is one of the most attractive ways to take inspiration from natural enzymes for the development of efficient catalytic systems.[11,12] SCNPs are composed of a single polymer chain and are generated by

---

[a] Organic Synthesis and Mass Spectrometry Laboratory, Center of Innovation and Research in Materials and Polymers (CIRMAP), University of Mons – UMONS, 23 Place du Parc, B-7000 Mons, Belgium. E-mail: pascal.gerbaux@umons.ac.be
[b] Center for Materials Science, School of Chemistry and Physics, Queensland University of Technology (QUT), 2 George Street, Brisbane, Queensland 4000, Australia. E-mail: christopher.barnerkowollik@qut.edu.au
[c] Laboratory for Chemistry of Novel Materials, Center of Innovation and Research in Materials and Polymers (CIRMAP), Materials Research Institute, University of Mons - UMONS, 23 Place du Parc, B-7000 Mons, Belgium
[d] Institute of Nanotechnology (INT) and Institute of Functional Interfaces (IFG), Karlsruhe Institute of Technology (KIT), Hermann-von-Helmholtz-Platz, 76344 Eggenstein-Leopoldshafen, Germany

† Electronic supplementary information (ESI) available. See DOI: https://doi.org/10.1039/d5py00194c

intramolecular interactions such as covalent bonds, even if weaker bonds have been employed such as coordination or supramolecular association.[13–15] Typically, the collapse of the polymer chain is induced by irreversible covalent[16–18] or reversible covalent (dynamic)[19] cross-linking processes.

SCNPs and their parent precursor polymers, however, are very challenging to characterize, due to the limitations of conventional characterization methods, *i.e.* NMR or IR spectroscopy as well as size-exclusion chromatography (SEC), to decipher the complex morphological arrangement and composition within the polymer coil in solution and – as examined herein – the gas phase. Furthermore, SCNPs and their parent polymer precursors cannot be crystallized like proteins and enzymes, eliminating the possibility of performing X-ray analysis.[20–22] For establishing the molecular structures of macromolecules including proteins, nucleic acids and synthetic polymers, mass spectrometry (MS) is now well acknowledged as an effective method.[23] The MS investigation of non-volatile macromolecules has become accessible with the advent of techniques such as electrospray ionization (ESI) and matrix-assisted laser desorption/ionization (MALDI).[24–30] While ESI is used less frequently to examine complex polymer mixtures,[31] MALDI remains the most commonly employed technique for single-stage MS structural characterization of polymers.[32–36] *Via* high-resolution MS, the nature of the (co)monomer units and end groups can be determined, whereas the arrangement of co-monomers within copolymers may sometimes be obtained by combining high-resolution mass spectrometry (HRMS) with mass spectrometry (MS) techniques.[37–40] Recently, ion mobility coupled to mass spectrometry (IMS-MS) has emerged as a promising tool for the study of (co)polymer architectures.[32,36,41–50] In IMS-MS experiments, ions move under the influence of an electric field through a mobility cell filled with a buffer gas, and their drift times are measured and converted into collisional cross sections (CCS_{exp}). Longer ion drift times correspond to larger ion CCS_{exp} as larger ions are exposed to more collisions and greater drag force than the compact ones (having smaller CCS_{exp}). As the internal structure of polymer ions cannot be determined from a unique CCS value, atomistic simulations are required to fully characterize polymer ions. In particular, ion structures obtained from fully atomistic molecular dynamics (MD) simulations in the gas phase that best represent the conformations sampled by IMS-MS are identified by comparing the experimental and theoretical CCS (CCS_{exp} *vs.* CCS_{th}).[41,46,49–58] The IMS-MS/MD combination provides an accurate description of the molecular structures of individual polymer chains and has already been widely used to characterize different types of polymers and polymer architectures.[37,41,51,55,57,59–64] Polymers are random coils in solution,[65,66] making the application of IMS-MS to examine their solution-phase structure challenging due to the transition from the condensed phase to the gas phase and the ionization processes that are known to affect the polymer chain geometry. On the other hand, since the collapse of SCNPs is underpinned by specific interactions within the prepolymer structure, (partial) structure conservation upon electrospray ionization may be envisioned, making IMS-MS/MD a promising structural characterization method for the parent precursor analysis and – ultimately – the SCNPs themselves.

Some of us have recently reported the synthesis and characterization of polystyrene-based gold-containing photoswitchable copolymers and their subsequent folding into SCNPs.[67] The chains were decorated with pendent phosphine ligands complexed with catalytically active gold motifs (AuCl units). ^1H nuclear magnetic resonance (NMR) spectroscopy and size exclusion chromatography (SEC) were used to characterize the pre-polymers and provide evidence for the formation of SCNPs.[67] In a bottom-up approach toward the use of IMS-MS/MD for prepolymer and ultimately SCNP characterization, we recently investigated the gas-phase structure of polystyrene ions with different end groups to establish how the nature and the rigidity of the monomer unit affect charge stabilization. We demonstrated that – in contrast to polar polymers, wherein the charges are located deep in the ionic globules – the charges in the PS ions are rather located at the periphery of the polymer backbone, leading to singly and doubly charged PS ions adopting dense, elliptic-shaped structures.[68]

In the present contribution, we move one step further towards detailed SCNP characterization using the IMS-MS/MD combination by examining in detail the conformation of gaseous Au-functionalized SCNP pre-copolymer ions containing three styrene derivatives, *i.e.* styrene, styrene-CH_2-OH and styrene-PPh_2-AuCl; see Scheme 1. The examined copolymer – with its chain distribution and statistical incorporation of the three monomer units – is a highly information-rich system, where each chain is part of a unique subset of identical chains, making it a highly worthwhile system to carefully

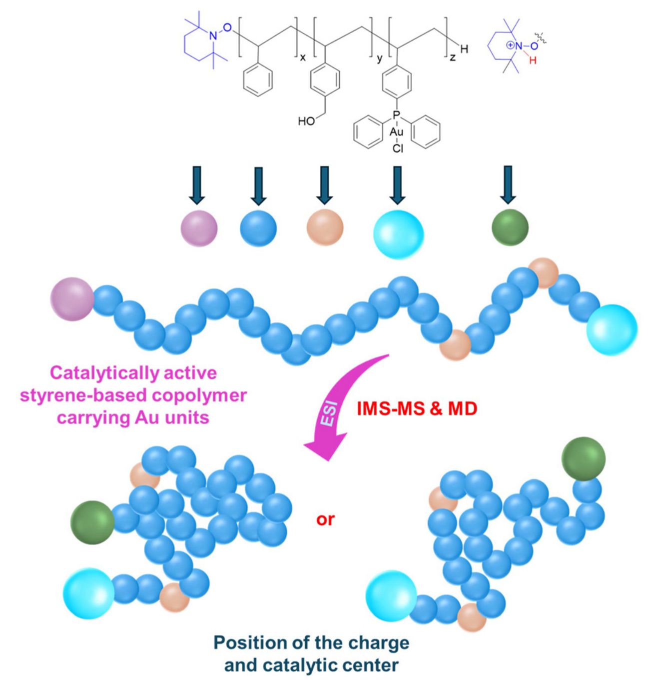

Scheme 1 Illustration of the folding of complex copolymer ions using the IMS-MS/MD approach.

characterize well beyond the standard analysis methodologies used for SCNP prepolymer analysis. We submit that, while the current analysis is conducted in the gas phase, important learnings about the copolymer structure can be deduced, including the all-important chain folding geometry. While the coil geometry in solution will certainly be affected by the solvent, gas-phase methods provide detailed insight into chain conformations. We believe that only *via* the combination of a range of analytical techniques applied to a specific polymer system – including both solution and gas phases – can an encompassing picture of its folding geometry be established. Finally, the current study does not seek to sequence each polymer chain to determine the order of the co-monomer units, but rather provides an overarching view of the composition information and folding for subsets of identical chains.

2. Experimental section

HPLC-grade tetrahydrofuran (>99.8%), acetonitrile (>99.9%) and acetone (>99.8%) solvents were purchased from Chem-Lab (Zedelgem, Belgium). Sodium iodide was purchased from VWR (Leuven, Belgium) and used for ESI-MS calibration. Polyethylene glycol was acquired from Sigma-Aldrich and utilized as an IMS-MS calibrant. TEMPO-(styrene)$_x$-(styrene-CH$_2$-OH)$_y$ (2,2,6,6-tetramethylpiperidine-*N*-oxyl end group – $Đ = 1.2$ – $M_n = 3200$ g mol^{-1}) and TEMPO-(styrene)$_x$-(styrene-CH$_2$-OH)$_y$-(styrene-PPh$_2$)$_w$-(styrene-PPh$_2$-AuCl)$_z$ (2,2,6,6-tetramethylpiperidine-*N*-oxyl end group – $Đ = 1.1$ – $M_n = 2400$ g mol^{-1}) were synthesized according to ref. 67. The ^{1}H NMR analyses and the SEC analyses of TEMPO-(styrene)$_x$-(styrene-CH$_2$-OH)$_y$ copolymers are collated in the ESI (refer to Fig. S1†). For the TEMPO-(styrene)$_x$-(styrene-CH$_2$-OH)$_y$-(styrene-PPh$_2$)$_w$-(styrene-PPh$_2$-AuCl)$_z$ copolymer, the ^{1}H NMR spectrum and the SEC data are presented in the ESI (refer to Fig. S2†).

2.1 Ion mobility experiments

1.0 mg mL^{-1} solutions of the copolymer were obtained by dissolving it in acetonitrile and tetrahydrofuran (80 : 20, v/v). The stock solutions were 100× diluted with acetonitrile and tetrahydrofuran (80 : 20, v/v) before ESI analysis. MS spectroscopy and CCS measurements were performed on a Waters Synapt G2-Si mass spectrometer. The solutions were infused at a flow rate of 5 μL min^{-1} with a capillary voltage of 3.1 kV, a source temperature of 100 °C and a desolvation temperature of 150 °C. The standard IMS-MS parameters were: wave height = 40 V, wave velocities = 350, 600 or 800 m s^{-1}, and mass range = m/z 50–4000; N$_2$ flow rate = 60 mL min^{-1}, He flow rate = 180 mL min^{-1} and trap bias = 45.0 V. A pre-established calibration procedure[69] was used to convert the experimentally determined arrival time distributions to $^{\mathrm{TW}}\mathrm{CCS}_{\mathrm{N2}\rightarrow\mathrm{He}}$,[70] which will be referred to as CCS$_{\mathrm{exp}}$.

2.2 Molecular dynamics (MD) simulations

All MD simulations were performed using Materials Studio software (BIOVIA, San Diego, CA).[71] For the TEMPO-(styrene)$_x$-(styrene-CH$_2$-OH)$_y$ copolymer, the PCFF was used and validated by the fact that the calculated effective density of TEMPO-polystyrene (0.62–0.66 Da Å^{-3}) is in good agreement with the reported density of bulk polystyrene (0.57–0.62 Da Å^{-3}).[68] For the TEMPO-(styrene)$_x$-(styrene-CH$_2$-OH)$_y$-(styrene-PPh$_2$-AuCl)$_z$ copolymer, we switched to the UFF since the parameters for gold are not available in PCFF. Both the PCFF and UFF were found to provide similar collisional cross sections for chains without styrene-PPh$_2$-AuCl units, thus validating our choice of using the UFF to model the behavior of polymer chains including the styrene-PPh$_2$-AuCl units. Force field assigned atomic charges were used for the simulations with the PCFF, while Gasteiger charges[72] were used in combination with the UFF. At first, geometry optimization was performed starting from a linear polymer chain (without charge). After adding a charge (H$^+$) to the optimized polymer chain, the geometry underwent additional optimization; the TEMPO group is chosen as the proton carrier due to the presence of the basic nitrogen atom.[68] Next, quenched dynamics (frames quenched every 5 ps) was run for 20 ns at 300 K, with a 1 fs timestep, and a cutoff of 100 Å for the van der Waals and electrostatic interactions. The most stable structure obtained from the quenched dynamics was then used as the starting point for a 25ns-long MD run (NVT ensemble; a constant number of particles, N, volume, V, and temperature ($T = 300$ K) and using a 1 fs time step). From this MD trajectory, 500 structures were extracted and used to obtain an average theoretical CCS$_{\mathrm{th}}$ computed using the trajectory method[73] (TM) model implemented within the Collidoscope software.[74]

2.3 Density functional theory (DFT) calculations

Density functional theory (DFT) calculations were performed using the Gaussian 09 (D01 revision)[75] suite to estimate the strength of the interactions between the fragments that interact through hydrogen bonding in the polymer.[76] In practice, the interaction energies have been estimated as the energy difference between the energy of the assembly made of the two interacting fragments and the energy of the isolated molecules. All the geometry optimization calculations were conducted using the B3LYP functional combined with the 6-31G** double zeta basis set for C, H, N, O, Cl, and P and the LANL2DZ basis set for gold.[77] To properly describe the dispersion interactions, Grimme's empirical dispersion correction GD3BJ was applied.[78] In all cases, the interaction energies have been corrected for the basis set superposition error (BSSE) through the use of the Counterpoise method.[79] Note that, in all DFT calculations, the complex structure of the macromolecules has not been considered, as only the two interacting fragments were taken into account.

3. Results and discussion

The copolymers, *i.e.* TEMPO-(styrene)$_x$-(styrene-CH$_2$-OH)$_y$ (M_n = 3200 g mol^{-1} and $Đ = 1.2$ determined *via* SEC) and TEMPO-

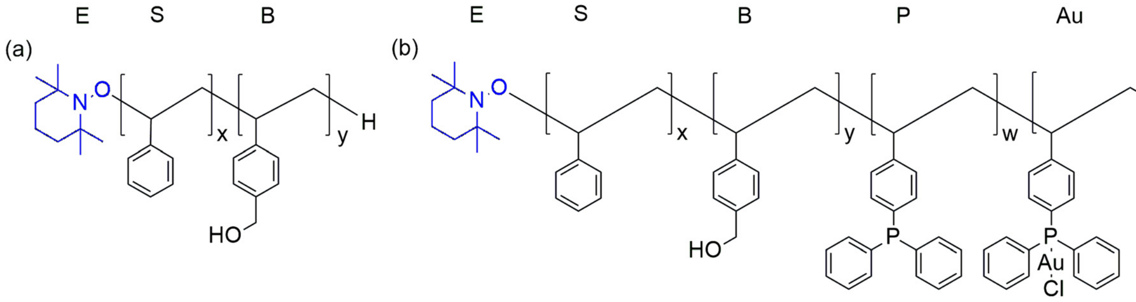

Scheme 2 The abbreviation used in the current study alongside the chemical structures of the selected copolymers: (a) TEMPO-(styrene)$_x$-(styrene-CH$_2$-OH)$_y$ and (b) TEMPO-(styrene)$_x$-(styrene-CH$_2$-OH)$_y$-(styrene-PPh$_2$-AuCl)$_w$-(styrene-PPh$_2$-AuCl)$_z$.

(styrene)$_x$-(styrene-CH$_2$-OH)$_y$-(styrene-PPh$_2$)$_w$-(styrene-PPh$_2$-AuCl)$_z$ (M_n = 2400 g mol^{-1} and $Đ$ = 1.1), are presented in Scheme 2. We defined the 2,2,6,6-tetramethylpiperidine-*N*-oxyl end group (TEMPO) as "E", the styrene residue as "S", and the styrene-CH$_2$-OH residue as "B", whereas "Au" is assigned to the styrene-PPh$_2$-AuCl moiety. Note that some free styrene-PPh$_2$ units were also detected and marked as "P". Herein, the degree of polymerization (DP) will be defined as the sum of the numbers of all different monomer units ($x + y + w + z$) in the copolymers.

3.1 ESI-MS analysis of the copolymers

Fig. 1 and 2 present the ESI mass spectra recorded for both copolymers. Singly charged ions (+1) are predominantly detected as proton adducts, such as [TEMPO-(styrene)$_x$-(styrene-CH$_2$-OH)$_y$ + H]$^+$ and [TEMPO-(styrene)$_x$-(styrene-CH$_2$-OH)$_y$-(styrene-PPh$_2$-AuCl)$_w$-(styrene-PPh$_2$-AuCl)$_z$ + H]$^+$. From Fig. 1, we observe that the TEMPO-(styrene)$_x$-(styrene-CH$_2$-OH)$_y$ copolymers are mostly detected as [E–S$_x$–B$_0$ + H]$^+$ (red circles), [E–S$_x$–B$_1$ + H]$^+$ (blue triangles) and [E–S$_x$–B$_2$ + H]$^+$ (green squares) ions. The ion compositions have been confirmed based on the measured *m*/*z* values and by comparison between experimental and simulated isotope patterns (refer to Fig. S3† for selected examples). Besides these dominant monomer combinations, less abundant ions with different compositions are also detected, typically [E–S$_x$–B$_{3\text{-}6}$ + H]$^+$.

The ESI-MS analysis of the second copolymer, *i.e.* TEMPO-(styrene)$_x$-(styrene-CH$_2$-OH)$_y$-(styrene-PPh$_2$)$_w$-(styrene-PPh$_2$-AuCl)$_z$, affords the more complex mass spectrum presented in Fig. 2. This copolymer is mostly detected as [E–S$_x$–B$_0$–P$_0$–Au$_0$ + H]$^+$ (purple triangles), [E–S$_x$–B$_0$–P$_0$–Au$_1$ + H]$^+$ (green stars), [E–S$_x$–B$_1$–P$_0$–Au$_1$ + H]$^+$ (red squares), and [E–S$_x$–B$_4$–P$_1$–Au$_0$ + H]$^+$ (blue circles) ions. The ion compositions have been confirmed based on the measured *m*/*z* values and by comparison between experimental and simulated isotope patterns (see Fig. S4 and 5† for selected examples). Besides these dominant monomer combinations, less abundant ions with different compositions are also detected, typically [E–S$_x$–B$_{1\text{-}2}$–P$_0$–Au$_{0\text{-}1}$ + H]$^+$, [E–S$_x$–B$_2$–P$_2$–Au$_0$ + H]$^+$ and [E–S$_x$–B$_4$–P$_1$–Au$_{0\text{-}1}$ + H]$^+$.

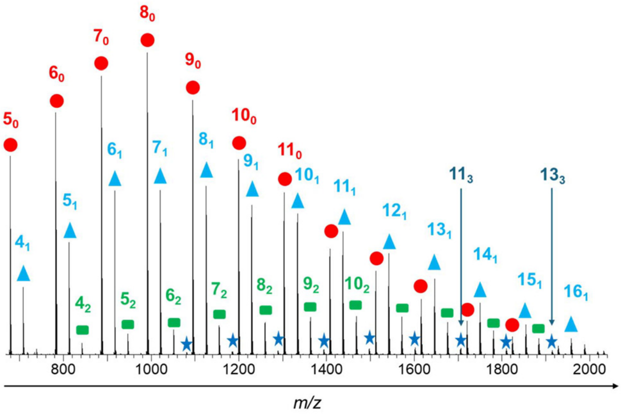

Fig. 1 ESI-MS mass spectrum of TEMPO-(styrene)$_x$-(styrene-CH$_2$-OH)$_y$ (0.01 mg mL^{-1}) in acetonitrile/tetrahydrofuran (80/20) (v/v). Red circles correspond to [E–S$_x$–B$_0$ + H]$^+$ ions (exemplified as x$_0$ in the figure), light blue triangles represent [E–S$_x$–B$_1$ + H]$^+$ ions (x_1), green squares correspond to [E–S$_x$–B$_2$ + H]$^+$ ions (x_2) and blue stars indicate [E–S$_x$–B$_3$ + H]$^+$ ions (x_3).

3.2 IMS-MS experiments on gaseous copolymer ions

Ion mobility experiments have been performed on all detected copolymer ions, and the experimental collisional cross sections (CCS$_{\text{exp}}$) have been determined. We further analyzed the symmetry of the arrival time distribution (ATD) for all ions to exclude the existence of non-interconverting gas phase structures (refer to Fig. S6† for selected examples). Facing the large dataset of determined CCS$_{\text{exp}}$, we decided to use the "CCS *vs.* DP" graphical representation (the so-called trend line analysis) for data visualization. Fig. S7a† presents the evolution of CCS$_{\text{exp}}$ *vs.* DP for the [E–S$_x$–B$_y$ + H]$^+$ ions (DP = x + y), whereas Fig. S7(b–f)† features the data for the detected [E–S$_x$–B$_y$–P$_w$–Au$_z$ + H]$^+$ ions (DP = $x + y + w + z$). From Fig. S6 and S7a,† for a given DP, we respectively observed that the impact of the copolymer sequence heterogeneity on the CCS$_{\text{exp}}$ is very limited and that the incorporation of 1 to 6 styrene-CH$_2$-OH residue(s) into the polymer backbone does not significantly influence the CCS$_{\text{exp}}$. For the second copolymer, *i.e.*, TEMPO-(styrene)$_x$-(styrene-CH$_2$-OH)$_y$-(styrene-PPh$_2$)$_w$-(styrene-PPh$_2$-AuCl)$_z$, the incorporation of styrene-PPh$_2$ and/or styrene-PPh$_2$-AuCl units

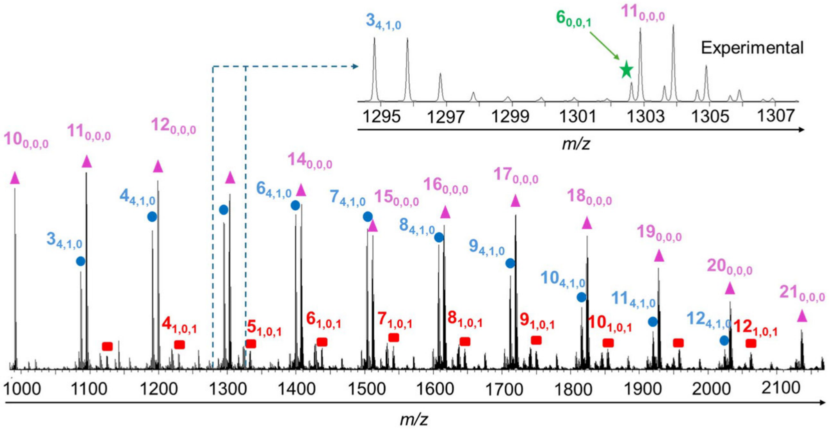

Fig. 2 ESI-MS mass spectra of TEMPO-(styrene)$_x$-(styrene-CH$_2$-OH)$_y$-(styrene-PPh$_2$)$_w$-(styrene-PPh$_2$-AuCl)$_z$ (0.01 mg mL^{-1}) in acetonitrile/tetrahydrofuran (80/20) (v/v). Blue circles correspond to $[E–S_x–B_4–P_1–Au_0 + H]^+$ ions (exemplified as $x_{4,1,0}$ in the figure), purple triangles represent $[E–S_x–B_0–P_0–Au_0 + H]^+$ ions ($x_{0,0,0}$), green stars correspond to $[E–S_x–B_0–P_0–Au_1 + H]^+$ ions ($x_{0,0,1}$) and red squares indicate $[E–S_x–B_1–P_0–Au_1 + H]^+$ ions ($x_{1,0,1}$).

into the copolymer backbone strongly impacts the CCS$_{exp}$ due to their bulkiness. Thus, it is challenging to establish the influence of these residues on the 3D structures, *i.e.* their folding, of the copolymer ions only based on the comparison of CCS$_{exp}$ and molecular modeling appears mandatory to generate candidate structures for an atomistic description of ion folding.

3.3 Molecular modeling and theoretical CCS calculations for $[E–S_x–B_y + H]^+$ ions

3.3.1. Impact of the copolymer sequence on the CCS. When investigating copolymers, the comonomer arrangement along the polymer backbone, *i.e.* their sequence, determines the behavior of individual chains; in the context of copolymer ion folding, the impact of the sequence on the ion CCS deserves to be discussed. From Fig. S6,† we can infer that the expected sequence heterogeneity for a given composition does not translate into broad or asymmetrical ATD characteristics of different ion structures. To further assess whether alternating, block or random copolymers behave differently upon ionization and desolvation, we generated two copolymers, namely $[E–S_6–B_6 + H]^+$ ions (DP = 12) and $[E–S_{12}–B_6 + H]^+$ ions (DP = 18) presenting higher proportions of B monomers than the detected ones (see Fig. 1). We executed MD simulations on a large diversity of hypothetical sequences and calculated the corresponding CCS$_{th}$. As shown in Fig. S8,† for the $[E–S_6–B_6 + H]^+$ ions and the $[E–S_{12}–B_6 + H]^+$ ions, the CCS$_{th}$ ranges expand from 365 to 385 Å^2 and from 455 to 490 Å^2, respectively. Since the CCS$_{FWHM}$ (FWHM stands for full width at half maximum – 50%) resolution of our Waters Synapt G2-Si is 40, *i.e.* $R_{CCS} = CCS/\Delta^{50\%}CCS = 40$, $\Delta^{50\%}CCS \sim 9$ and ~12 Å^2 would characterize the CCS distribution for both ion compositions, respectively. When analyzing Fig. S8,† we predict that for the considered hypothetical copolymer ions, the Waters Synapt G2-Si mass spectrometer would be able to discriminate different sequences, even if most of the different sequences will be hidden under a given CCS distribution centered at ~375 and 475 Å^2, for the $[E–S_6–B_6 + H]^+$ ions and the $[E–S_{12}–B_6 + H]^+$ ions, respectively.

To obtain atomistic insights into our experimental results, we selected one specific copolymer composition ($[E–S_{22}–B_1 + H]^+$ ions (*m/z* 2581.6)) for theoretical modelling and created three different sequences, namely $E–B_1–S_{22}$, $E–S_{11}–B_1–S_{11}$ and $E–S_{22}–B_1$. In these sequences, the alcohol moiety is positioned close to the TEMPO end group, in the middle of the chain and at the end of the chain, respectively. CCS$_{exp}$ has also been measured around 540 Å^2 with a $\Delta^{50\%}$CCS of ~ 17 Å^2 and an R_{CCS} of ~ 32, as shown in Fig. 3. The MD geometries are characterized by CCS$_{th}$ at 530 ± 8, 543 ± 8 and 554 ± 7 Å^2, respectively, for the $E–S_{11}–B_1–S_{11}$, $E–S_{22}–B_1$ and $E–B_1–S_{22}$ ions. Interestingly, the sequences with the styrene-CH$_2$-OH moiety lying away from the TEMPO end group fit the experimental values, whereas the $[E–B_1–S_{22} + H]^+$ ions appear less folded, *i.e.* with a higher CCS.

From the MD simulations (refer to Fig. 3), we detected strong H-bonds between protonated TEMPO (H atom) and the styrene-CH$_2$-OH group (O atom) for the more compact $E–S_{11}–B_1–S_{11}$ (3b) (1.69 Å ± 0.11 Å) and $E–S_{22}–B_1$ (3c) ions (1.60 Å ± 0.08 Å), whereas this H-bond is not present when the styrene-CH$_2$-OH group is directly attached to the TEMPO initiator in the $E–B_1–S_{22}$ ions (3d) (4.96 Å ± 0.40 Å). The strong H-bonds between the protonated TEMPO and the styrene-CH$_2$-OH group have also been measured for other copolymer compositions that have been experimentally identified (refer to Fig. S9 and Fig. S10†). This has been confirmed on model systems using Density Functional Theory (DFT) calculations that point to a hydrogen bond length of 1.81 Å and an interaction energy between the two subunits involved in the hydrogen bond of 8.1 kcal mol^{-1}.

We further subjected all detected $[E–S_x–B_1 + H]^+$ ions to MD simulations by selecting the $E–S_x–B_1$ sequence, *i.e.*, with the styrene-CH$_2$-OH group at the end of the copolymer chain. As

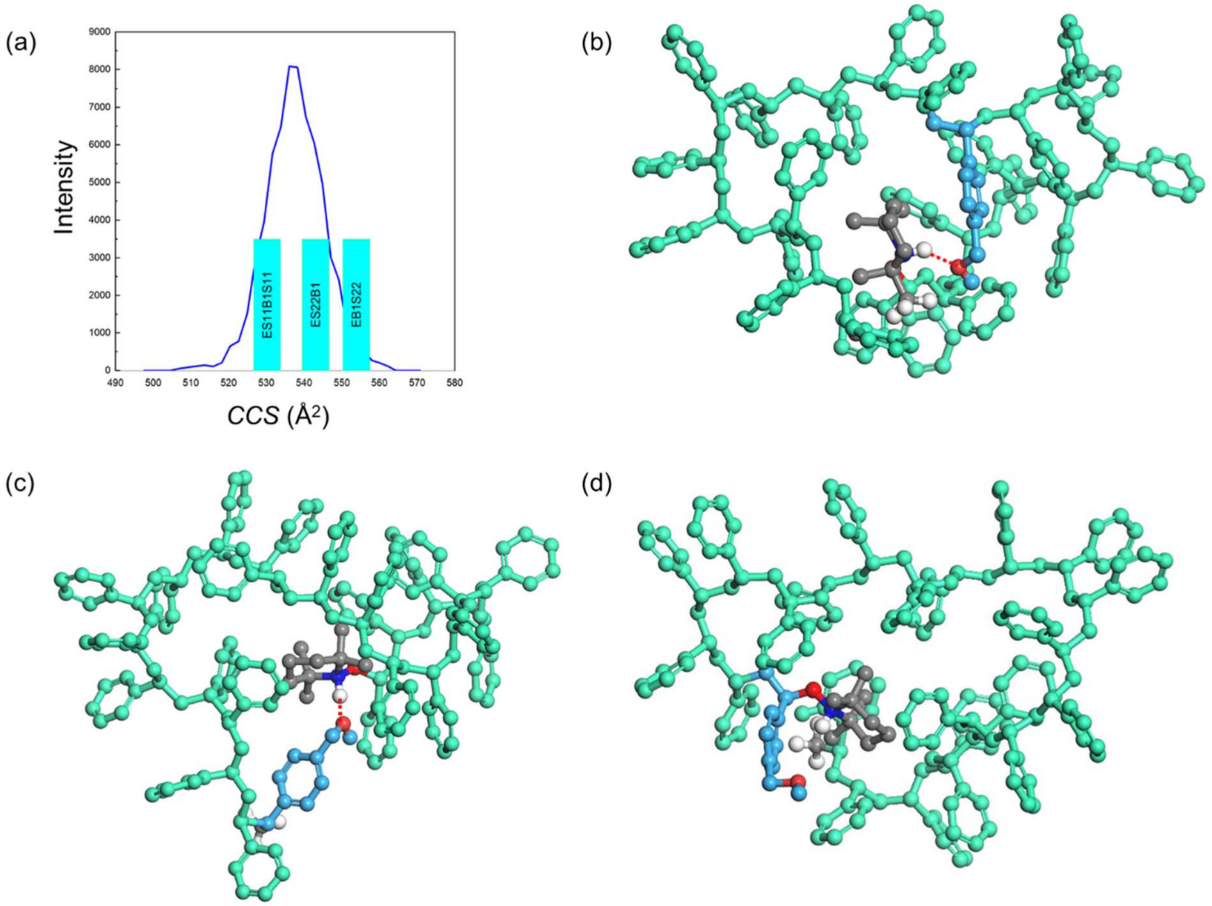

Fig. 3 Ion mobility mass spectrometry analysis and molecular dynamics simulations of [TEMPO-(styrene)$_{22}$-(styrene-CH$_2$-OH)$_1$ + H]$^+$ ions presenting three different sequences, namely E–S$_{11}$–B$_1$–S$_{11}$, E–S$_{22}$–B1 and E–B$_1$–S$_{22}$: (a) experimental CCS distribution and theoretical CCS$_{th}$ for the [M + H]$^+$ ions; (b–d) snapshots of the last frame of the MD simulations for (b) E–S$_{11}$–B$_1$–S$_{11}$ (CCS$_{th}$ = 530 Å^2), (c) E–S$_{22}$–B$_1$ (CCS$_{th}$ = 543 Å^2) and (d) E–B$_1$–S$_{22}$ (CCS$_{th}$ = 554 Å^2) ions.

featured in Fig. S11,† we found an excellent agreement between CCS$_{th}$ and CCS$_{exp}$ over the whole investigated mass range (m/z = 750–2750), allowing us to propose the optimized geometries as promising candidates for the detected ions. In our previous study related to TEMPO-initiated polystyrene (PS) ions, we reported that the folding of the PS rigid chain is controlled by phenyl ring interactions with the charge ultimately remaining excluded from the core of the globular ions. From the structures presented in Fig. 3, we observe that protonated TEMPO is associated with the styrene-CH$_2$-OH group through a strong H-bond. To better understand its effect on the structure of the copolymer, the distance between the charged center (protonated TEMPO) and the center-of-mass of the ion has been divided by the radius of gyration (R_g) for all [E–S$_x$–B$_1$ + H]$^+$ ions (x = 5–22) to generate normalized data for increasing DP (=x + 1). As shown in Fig. 4, the normalized distance is ∼0.8 for DP = 6 and decreases continuously upon chain elongation to reach ∼0.3 for DP = 23, revealing that, when an H-bond is present, the charged end group is progressively integrated at the center of the ions (refer to Fig. 4) with increasing DP.

In our previous report on the gas-phase structure of PS ions,[68] we used MD simulations to demonstrate that the folding of the PS rigid chain is induced by phenyl ring interactions, with the charge ultimately remaining excluded from the core of the globular ions, whereas the folding of polyether ions is initiated by the folding of the flexible polyether chain around the sodium ion that remains deeply settled in the core of the ions. The data of Fig. 4, *i.e.* polymer ions with the charge remaining localized in the core of the ions upon DP increase, prompted us to examine frame-by-frame MD trajectories for the E–S$_{22}$–B$_1$, E–B$_1$–S$_{22}$ and E–S$_{11}$–B$_1$–S$_{11}$ ions. As shown in Fig. 5 and S12,† the chain folding again appears to be triggered by the phenyl ring interactions for all ions. For the more compact [E–S$_{22}$–B$_1$ + H]$^+$ (CCS$_{th}$ = 543 Å^2) and [E–S$_{11}$–B$_1$–S$_{11}$ + H]$^+$ (CCS$_{th}$ = 530 Å^2) ions, the formation of an H-bond between protonated TEMPO and styrene-CH$_2$-OH further stabilizes them in the core of the globular ions; see Fig. 5 for a typical example. However, for the less compact [E–B$_1$–S$_{22}$ + H]$^+$ (CCS$_{th}$ = 554 Å^2) ions (refer to Fig. S12b†), the direct proximity of the TEMPO end group and the styrene-CH$_2$-OH first residue does not allow the for-

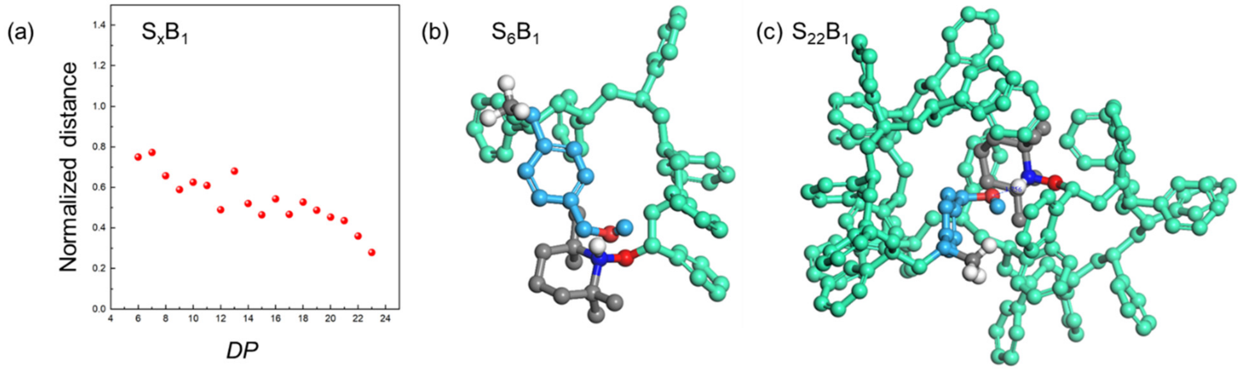

Fig. 4 Molecular dynamics simulations (PCFF force field, 298 K, 25 ns) of [TEMPO-(styrene)$_x$-(styrene-CH$_2$-OH)$_1$ + H]$^+$ions: (a) the evolution of the distance between the charged center and the center-of-mass (COM) normalized by the ion radius of gyration (R_g) that is marked by the normalized distance. (b) A snapshot of the last frame of the MD for [TEMPO-(styrene)$_6$-(styrene-CH$_2$-OH)$_1$ + H]$^+$ ions (DP = 7). (c) A snapshot of the last frame of the MD for [TEMPO-(styrene)$_{22}$-(styrene-CH$_2$-OH)$_1$ + H]$^+$ ions (DP = 23).

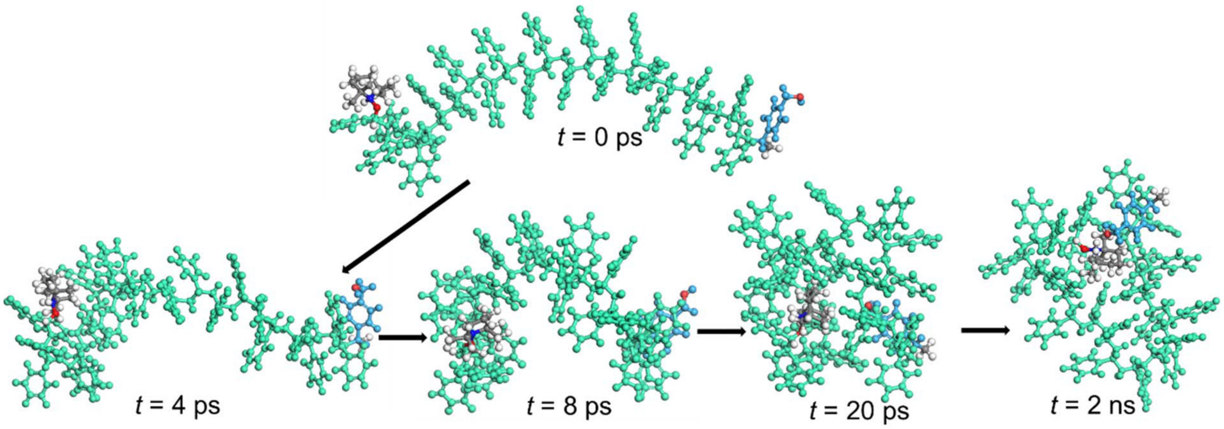

Fig. 5 Molecular dynamics simulations (PCFF force field, 300 K, 2 ns) of [E–S$_{22}$–B$_1$ + H]$^+$ ions (DP = 23): snapshots at different times of the trajectory revealing that the folding process is mostly initiated by π–π interactions between phenyl rings with the H-bonded protonated TEMPO and styrene-CH$_2$-OH, ultimately incorporated into the core of the equilibrated structure. The styrene-CH$_2$-OH and the TEMPO residues are highlighted in grey and blue for visualization.

mation of an H-bond so that the protonated TEMPO remains at the surface of the globular ion.

3.4 Molecular modeling and theoretical CCS calculations for [E–S$_x$–B$_y$-Au$_z$ + H]$^+$ ions

In our bottom-up approach, we further examined the selected TEMPO-(styrene)$_x$-(styrene-CH$_2$-OH)$_y$-(styrene-PPh$_2$-AuCl)$_z$ copolymer ions *via* our IMS-MS/MD approach, namely the [E–S$_x$–B$_y$–Au$_z$ + H]$^+$ ions detected in the ESI mass spectrum presented in Fig. 2. PCFF was used in our previous study[68] and in the first section of this study. However, due to the absence of the Au descriptors in the PCFF, we turned to the universal force field (UFF) for the TEMPO-(styrene)$_x$-(styrene-CH$_2$-OH)$_y$-(styrene-PPh$_2$-AuCl)$_z$ copolymer ions. As described in the ESI (Fig. S13†), we tested whether the UFF was able to reproduce CCS$_{exp}$ and CCS$_{PCFF}$ by calculating, using both the UFF and the PCFF, CCS$_{th}$ for TEMPO-initiated polystyrene homopolymer ions (DP = 8–17) and TEMPO-initiated styrene/styrene-CH$_2$-OH copolymer ions (DP = 8–19). Since the three different CCSs, *i.e.* CCS$_{exp}$, CCS$_{UFF}$ and CCS$_{PCFF}$, are nearly identical over the investigated DP ranges for both copolymer ions, we consider that both force fields are able to generate reliable molecular structures without any further validation/parametrization.

We were thus interested in the comparison between the [E–S$_x$–B$_1$–Au$_0$ + H]$^+$ (Fig. 1) and the [E–S$_x$–B$_0$–Au$_1$ + H]$^+$ (green stars in Fig. 2) ions to determine the impact of the bulky Au-containing group on the ion structure. To start our MD simulations, we created [E–S$_x$–B$_0$–Au$_1$ + H]$^+$ input structures by positioning the gold-containing residue at the end of the PS backbone, *i.e.* by formally replacing the styrene-CH$_2$-OH group within the [E–S$_x$–B$_1$–Au$_0$ + H]$^+$ ions. As shown in Fig. 6a, for both ion series, CCS$_{exp}$ and CCS$_{th}$ are nicely fitting. Obviously, the CCSs of the Au-containing ions are larger for a given DP due to the presence of the bulky triphenylphosphine ligand.

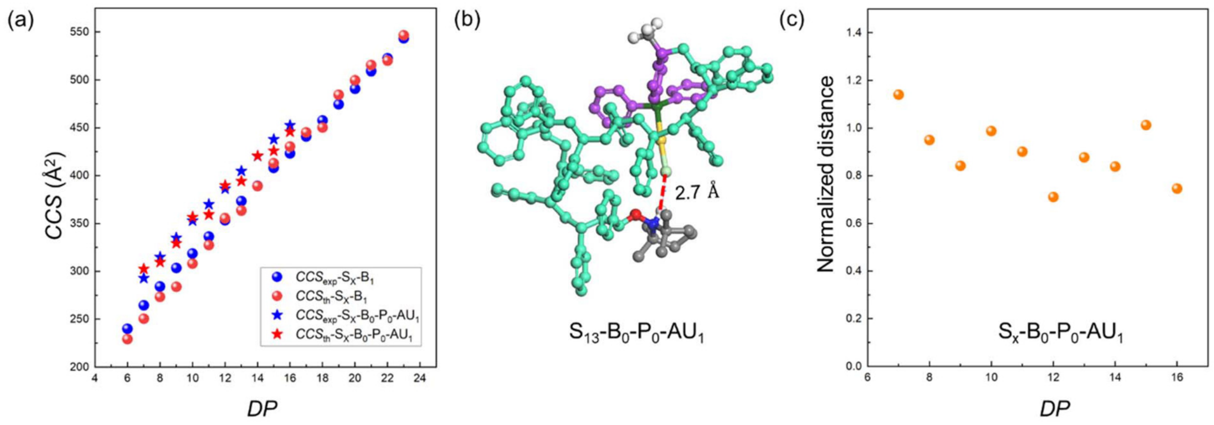

Fig. 6 Ion mobility mass spectrometry analysis and molecular dynamics simulations (UFF/PCFF, 298 K, 25 ns) of $[E-S_x-B_1 + H]^+$ (PCFF) and $[E-S_x-Au_1 + H]^+$ ions (UFF): (a) comparison between CCS_{exp} and CCS_{th} over the full DP range, (b) snapshot of the last frame of the MD (UFF, 298 K, 25 ns) for $[E-S_{13}-Au_1 + H]^+$ ions revealing the presence of an H-bond between protonated TEMPO and the chlorine atom of the triphenylphosphine-AuCl moiety, and (c) the evolution of the distance between the charged center and the center-of-mass (COM) normalized by the ion radius of gyration (R_g), which is marked by the normalized distance.

As featured in Fig. 6b, for the specific case of the $[E-S_{13}-Au_1 + H]^+$ ions, an H-bond is formed between the protonated TEMPO end group and the chlorine atom of the distal triphenylphosphine-AuCl moiety (see Fig. S14†), hereby linking both ends of the polymer backbone. This is reminiscent of the styrene/styrene-CH_2-OH case, except that the N–H⋯O–H bond is here replaced by an N–H⋯Cl bond. A second difference is the position of the charged center in the globular ions. Indeed, as shown in Fig. 6c, from DP = 7 to 16, the charged center remains at the surface of the ion globule because of the steric hindrance created by the PPh_3 unit, which prevents the charged center from getting incorporated into the center of the globular ion, as also sketched in Fig. 6b. MD simulations indicate that the H-bond distance remains between 2.5 and

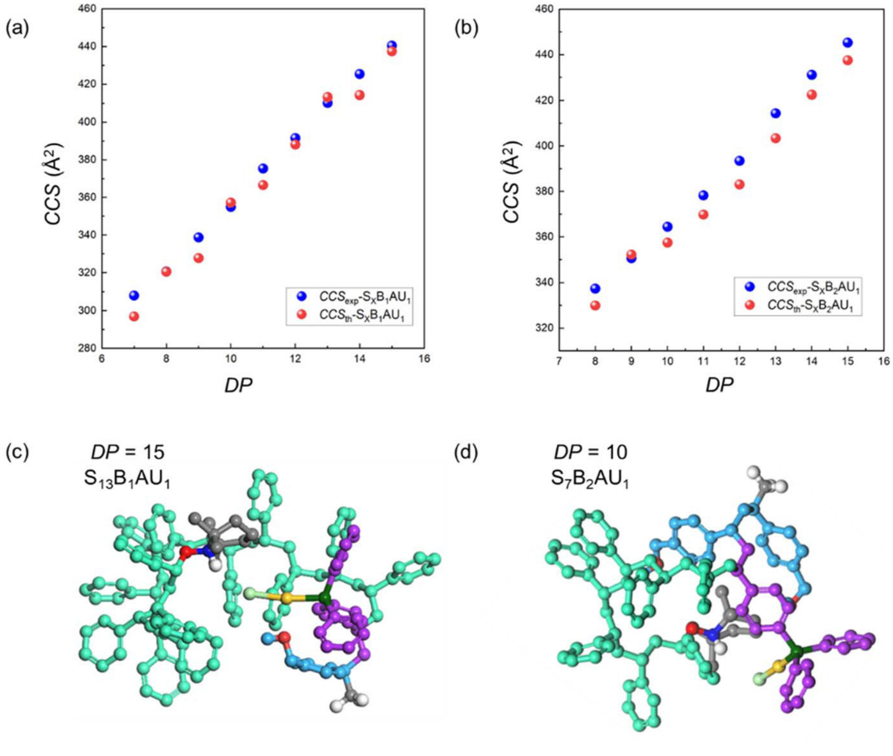

Fig. 7 Ion mobility mass spectrometry analysis and molecular dynamics simulations of $[E-S_x-B_1-Au_1 + H]^+$ and $[E-S_x-B_2-Au_1 + H]^+$ ions: (a and b) comparison between CCS_{exp} and CCS_{th} over the full DP range, and (c and d) snapshots of the last frame of the MD (UFF, 298 K, 25 ns) for $[E-S_{13}-B_1-Au_1 + H]^+$ and $[E-S_7-B_2-Au_1 + H]^+$ ions, respectively.

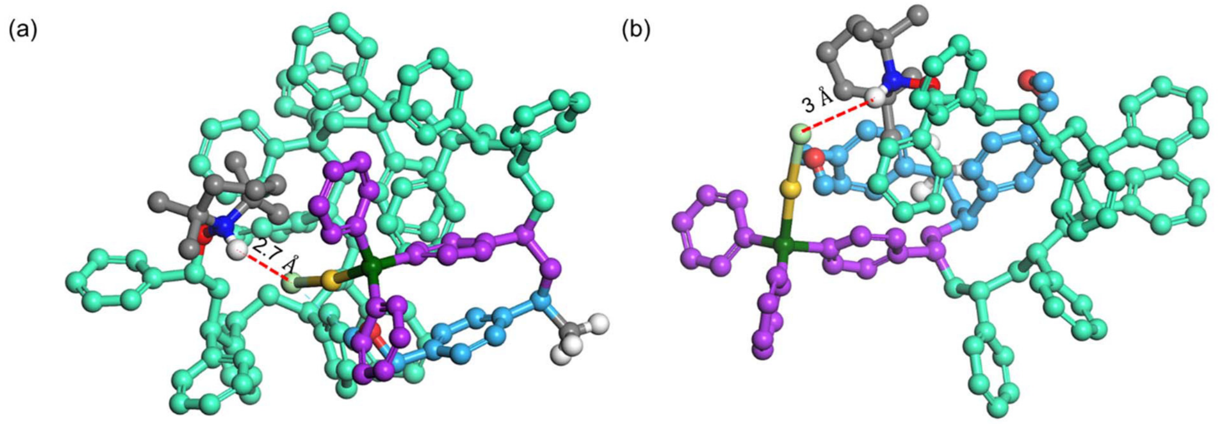

Fig. 8 Molecular dynamics simulations (UFF, 298 K, 25 ns) of [TEMPO-(styrene)$_x$-(styrene-CH$_2$-OH)$_y$-(styrene-PPh$_2$-AuCl)$_z$ + H]$^+$ions, and snapshot of the last frame of the MD: (a) DP = 15 (x = 13, y = 1, and z = 1) and (b) DP = 10 (x = 7, y = 2, and z = 1), where the hydrogen bond and the bonding distance are represented in red. Here, the styrene monomer unit is indicated in dark green, the styrene-CH$_2$-OH is indicated in light blue, styrene-PPh$_2$ is indicated in plum and the end group is indicated in grey.

3 Å (refer to Fig. S15†). We also calculated this H-bond length using the same DFT approach on model systems as before, except that the gold atom is described using the LANL2DZ basis set. The average N–H⋯Cl H-bond length amounts to 2.2 Å, and the corresponding interaction energy between the styrene-PPh$_2$-AuCl and the protonated TEMPO units was estimated to be 15.4 kcal mol^{-1}, twice that calculated for the styrene-CH$_2$-OH/TEMPO interaction (8.12 kcal mol^{-1}).

As shown in Fig. 2, copolymer ions combining the three different monomers, *i.e.* styrene, styrene-CH$_2$-OH and styrene-PPh$_2$-AuCl, were also detected upon ESI analysis, with the specific case of $[\mathrm{E{-}S}_x\mathrm{{-}B}_y\mathrm{{-}Au}_1 + \mathrm{H}]^+$ ions (y = 1 and 2). We determined their CCS$_{\text{exp}}$ and CCS$_{\text{th}}$, which are compared in Fig. 7, and once again observed excellent agreement between the experimental and theoretical values.

The hydroxyl/chloride groups of the styrene-CH$_2$-OH/styrene-PPh$_2$-AuCl monomer units are thus H-bonded with protonated TEMPO (NH group) *via* the charged center (see Fig. 8). When the chlorine atom, rather than the hydroxyl group, is involved in a hydrogen bond, the DFT results demonstrate that the ion is significantly more stabilized. Depending on the composition, there may also be additional weak hydrogen bonds (refer to Fig. S14†).

4. Conclusions

The macromolecular architecture and coil folding of gaseous polystyrene-based complex precopolymer ions have been examined using molecular dynamics simulations in conjunction with IMS-MS as a step toward SCNP characterization. We determine the conformation of gaseous Au-functionalized copolymer ions consisting of three different monomer units in detail, *i.e.* styrene, styrene-CH$_2$-OH and styrene-PPh$_2$-AuCl. All copolymers were prepared *via* nitroxide-mediated radical polymerization (NMP) using TEMPO as the initiator. All copolymer ions corresponded to $[\mathrm{M} + \mathrm{H}]^+$ ions with the proton anchored on the nitrogen atom of the TEMPO end group.

The styrene/styrene-CH$_2$-OH ions were shown to be stabilized by a strong H-bond established between protonated TEMPO and the oxygen atom of the styrene-CH$_2$-OH group, and the charge center gradually migrates from the surface of the ion structure toward the center of the ion aggregate as the DP increases. On the other hand, an N–H⋯Cl H-bond, linking protonated TEMPO to the chlorine atom, was also detected *via* MD simulations and confirmed through DFT calculations for styrene/styrene-CH$_2$-OH/styrene-PPh$_2$-AuCl ions. Due to the steric hindrance of the PPh$_3$ unit, the charge center of the gold copolymer remains at the surface of the globular ions, pointing to a strong impact of the chemical structure of the subunits on the three-dimensional conformation of the SNCP prepolymers and hence on their resulting properties. The next step is the analysis of the folded SCNPs *via* the methodology described herein, which includes a comparison of their catalytic ability in varying solvent environments beyond the single solvent assessed in our earlier study.[67]

Data availability

The data supporting this article have been included as part of the ESI†.

Conflicts of interest

There are no conflicts to declare.

Acknowledgements

The S^{2}MOs lab is grateful to the "Fonds National de la Recherche Scientifique (FRS-FNRS)" for financial support for the acquisition of the Waters Synapt G2-Si mass spectrometer. SN thanks UMONS and QUT for his PhD thesis grant. Computational resources have been provided by the Consortium des Équipements de Calcul Intensif (CÉCI), funded by the Fonds de la Recherche Scientifique de Belgique (F.R.S.-FNRS) under Grant No. 2.5020.11 and by the Walloon Region (ZENOBE and LUCIA Tier-1 supercomputers). Q. D. and J. C. are FNRS research fellows. C. B.-K. and S. B. acknowledge continued support from the Queensland University of Technology (QUT) and its Centre for Materials Science.

References

1 R. A. Copeland, *Enzymes: A Practical Introduction to Structure, Mechanism, and Data Analysis*, Wiley, 1st edn, 2000.
2 T. Yamamoto, T. Yamada, Y. Nagata and M. Suginome, *J. Am. Chem. Soc.*, 2010, **132**, 7899–7901.
3 K. Inoue, *Prog. Polym. Sci.*, 2000, **25**, 453–571.
4 R. Breslow and S. D. Dong, *Chem. Rev.*, 1998, **98**, 1997–2012.
5 C. Liang and J. M. J. Fréchet, *Prog. Polym. Sci.*, 2005, **30**, 385–402.
6 A. Sanchez-Sanchez, A. Arbe, J. Colmenero and J. A. Pomposo, *ACS Macro Lett.*, 2014, **3**, 439–443.
7 Y. Bai, X. Feng, H. Xing, Y. Xu, B. K. Kim, N. Baig, T. Zhou, A. A. Gewirth, Y. Lu, E. Oldfield and S. C. Zimmerman, *J. Am. Chem. Soc.*, 2016, **138**, 11077–11080.
8 R. Breslow, *Acc. Chem. Res.*, 1995, **28**, 146–153.
9 I. Guzman and M. Gruebele, *J. Phys. Chem. B*, 2014, **118**, 8459–8470.
10 D. M. Mitrea and R. W. Kriwacki, *FEBS Lett.*, 2013, **587**, 1081–1088.
11 I. Perez-Baena, F. Barroso-Bujans, U. Gasser, A. Arbe, A. J. Moreno, J. Colmenero and J. A. Pomposo, *ACS Macro Lett.*, 2013, **2**, 775–779.
12 H. Rothfuss, N. D. Knöfel, P. W. Roesky and C. Barner-Kowollik, *J. Am. Chem. Soc.*, 2018, **140**, 5875–5881.
13 E. J. Foster, E. B. Berda and E. W. Meijer, *J. Am. Chem. Soc.*, 2009, **131**, 6964–6966.
14 N. Hosono, M. A. J. Gillissen, Y. Li, S. S. Sheiko, A. R. A. Palmans and E. W. Meijer, *J. Am. Chem. Soc.*, 2013, **135**, 501–510.
15 O. Altintas and C. Barner-Kowollik, *Macromol. Rapid Commun.*, 2012, **33**, 958–971.
16 E. Harth, B. V. Horn, V. Y. Lee, D. S. Germack, C. P. Gonzales, R. D. Miller and C. J. Hawker, *J. Am. Chem. Soc.*, 2002, **124**, 8653–8660.
17 D. Mecerreyes, V. Lee, C. J. Hawker, J. L. Hedrick, A. Wursch, W. Volksen, T. Magbitang, E. Huang and R. D. Miller, *Adv. Mater.*, 2001, **13**, 204–208.
18 T. E. Dukette, M. E. Mackay, B. Van Horn, K. L. Wooley, E. Drockenmuller, M. Malkoch and C. J. Hawker, *Nano Lett.*, 2005, **5**, 1704–1709.
19 B. S. Murray and D. A. Fulton, *Macromolecules*, 2011, **44**, 7242–7252.
20 E. Jurneczko and P. E. Barran, *Analyst*, 2011, **136**, 20–28.
21 A. McPherson and J. A. Gavira, *Acta Crystallogr., Sect. F: Struct. Biol. Commun.*, 2014, **70**, 2–20.
22 K. A. Kantardjieff and B. Rupp, *Protein Sci.*, 2003, **12**, 1865–1871.
23 J. Steinkoenig, H. Rothfuss, A. Lauer, B. T. Tuten and C. Barner-Kowollik, *J. Am. Chem. Soc.*, 2017, **139**, 51–54.
24 T. Nohmi and J. B. Fenn, *J. Am. Chem. Soc.*, 1992, **114**, 3241–3246.
25 J. B. Fenn, *Angew. Chem., Int. Ed.*, 2003, **42**, 3871–3894.
26 C. S. Kaddis, S. H. Lomeli, S. Yin, B. Berhane, M. I. Apostol, V. A. Kickhoefer, L. H. Rome and J. A. Loo, *J. Am. Soc. Mass Spectrom.*, 2007, **18**, 1206–1216.
27 M. T. Marty, H. Zhang, W. Cui, R. E. Blankenship, M. L. Gross and S. G. Sligar, *Anal. Chem.*, 2012, **84**, 8957–8960.
28 J. Marcoux and C. V. Robinson, *Structure*, 2013, **21**, 1541–1550.
29 K. Tanaka, H. Waki, Y. Ido, S. Akita, Y. Yoshida, T. Yoshida and T. Matsuo, *Rapid Commun. Mass Spectrom.*, 1988, **2**, 151–153.
30 M. Karas and F. Hillenkamp, *Anal. Chem.*, 1988, **60**, 2299–2301.
31 T. Nitsche, J. Steinkoenig, K. De Bruycker, F. R. Bloesser, S. J. Blanksby, J. P. Blinco and C. Barner-Kowollik, *Macromolecules*, 2019, **52**, 2597–2606.
32 J. N. Hoskins, S. Trimpin and S. M. Grayson, *Macromolecules*, 2011, **44**, 6915–6918.
33 C. Wesdemiotis, *Angew. Chem., Int. Ed.*, 2017, **56**, 1452–1464.
34 G. Montaudo, F. Samperi and M. S. Montaudo, *Prog. Polym. Sci.*, 2006, **31**, 277–357.
35 T. Josse, J. De Winter, P. Dubois, O. Coulembier, P. Gerbaux and A. Memboeuf, *Polym. Chem.*, 2015, **6**, 64–69.
36 C. D. Foley, B. Zhang, A. M. Alb, S. Trimpin and S. M. Grayson, *ACS Macro Lett.*, 2015, **4**, 778–782.
37 A. T. Jackson, J. H. Scrivens, J. P. Williams, E. S. Baker, J. Gidden and M. T. Bowers, *Int. J. Mass Spectrom.*, 2004, **238**, 287–297.
38 C. N. McEwen and P. M. Peacock, *Anal. Chem.*, 2002, **74**, 2743–2748.
39 S. M. Weidner and S. Trimpin, *Anal. Chem.*, 2008, **80**, 4349–4361.
40 K. Ito, S. Kitagawa and H. Ohtani, *Anal. Sci.*, 2019, **35**, 169–174.
41 J. Gidden, T. Wyttenbach, A. T. Jackson, J. H. Scrivens and M. T. Bowers, *J. Am. Chem. Soc.*, 2000, **122**, 4692–4699.
42 K. Kim, J. W. Lee, T. Chang and H. I. Kim, *J. Am. Soc. Mass Spectrom.*, 2014, **25**, 1771–1779.
43 J. L. Fischer, C. A. Lutomski, T. J. El-Baba, B. N. Siriwardena-Mahanama, S. M. Weidner, J. Falkenhagen, M. J. Allen and S. Trimpin, *J. Am. Soc. Mass Spectrom.*, 2015, **26**, 2086–2095.

44 D. Bagal, H. Zhang and P. D. Schnier, *Anal. Chem.*, 2008, **80**, 2408–2418.

45 S. Trimpin and D. E. Clemmer, *Anal. Chem.*, 2008, **80**, 9073–9083.

46 D. Morsa, T. Defize, D. Dehareng, C. Jérôme and E. De Pauw, *Anal. Chem.*, 2014, **86**, 9693–9700.

47 C. Barrère, W. Selmi, M. Hubert-Roux, T. Coupin, B. Assumani, C. Afonso and P. Giusti, *Polym. Chem.*, 2014, **5**, 3576–3582.

48 S. Crotty, S. Gerişlioğlu, K. J. Endres, C. Wesdemiotis and U. S. Schubert, *Anal. Chim. Acta*, 2016, **932**, 1–21.

49 Q. Duez, S. Moins, O. Coulembier, J. De Winter, J. Cornil and P. Gerbaux, *J. Am. Soc. Mass Spectrom.*, 2020, **31**, 2379–2388.

50 Q. Duez, S. Hoyas, T. Josse, J. Cornil, P. Gerbaux and J. De Winter, *Mass Spectrom. Rev.*, 2023, **42**, 1129–1151.

51 J. Gidden, T. Wyttenbach, J. J. Batka, P. Weis, A. T. Jackson, J. H. Scrivens and M. T. Bowers, *J. Am. Soc. Mass Spectrom.*, 1999, **10**, 883–895.

52 J. Gidden, M. T. Bowers, A. T. Jackson and J. H. Scrivens, *J. Am. Soc. Mass Spectrom.*, 2002, **13**, 499–505.

53 G. Von Helden, T. Wyttenbach and M. T. Bowers, *International Journal of Mass Spectrometry and Ion Processes*, 1995, **146–147**, 349–364.

54 T. Wyttenbach, G. Von Helden and M. T. Bowers, *International Journal of Mass Spectrometry and Ion Processes*, 1997, **165–166**, 377–390.

55 J. De Winter, V. Lemaur, R. Ballivian, F. Chirot, O. Coulembier, R. Antoine, J. Lemoine, J. Cornil, P. Dubois, P. Dugourd and P. Gerbaux, *Chem. – Eur. J.*, 2011, **17**, 9738–9745.

56 S. Trimpin, M. Plasencia, D. Isailovic and D. E. Clemmer, *Anal. Chem.*, 2007, **79**, 7965–7974.

57 C. Larriba and J. Fernandez De La Mora, *J. Phys. Chem. B*, 2012, **116**, 593–598.

58 J. R. N. Haler, V. Lemaur, J. Far, C. Kune, P. Gerbaux, J. Cornil and E. De Pauw, *J. Am. Soc. Mass Spectrom.*, 2020, **31**, 633–641.

59 J. Song, C. H. Grün, R. M. A. Heeren, H. Janssen and O. F. van den Brink, *Angew. Chem., Int. Ed.*, 2010, **49**, 10168–10171.

60 F. Maire, G. Coadou, L. Cravello and C. M. Lange, *J. Am. Soc. Mass Spectrom.*, 2013, **24**, 238–248.

61 J. Gidden, M. T. Bowers, A. T. Jackson and J. H. Scrivens, *J. Am. Soc. Mass Spectrom.*, 2002, **13**, 499–505.

62 T. Gruendling, S. Weidner, J. Falkenhagen and C. Barner-Kowollik, *Polym. Chem.*, 2010, **1**, 599.

63 S. Lee, T. Wyttenbach and M. T. Bowers, *International Journal of Mass Spectrometry and Ion Processes*, 1997, **167–168**, 605–614.

64 J. Gidden, A. T. Jackson, J. H. Scrivens and M. T. Bowers, *Int. J. Mass Spectrom.*, 1999, **188**, 121–130.

65 M. L. Alessi, A. I. Norman, S. E. Knowlton, D. L. Ho and S. C. Greer, *Macromolecules*, 2005, **38**, 9333–9340.

66 A. E. Tonelli, *Macromolecules*, 2014, **47**, 6141–6143.

67 A. E. Izuagbe, V. X. Truong, B. T. Tuten, P. W. Roesky and C. Barner-Kowollik, *Macromolecules*, 2022, **55**, 9242–9248.

68 S. Naskar, A. Minoia, Q. Duez, A. Izuagbe, J. De Winter, S. J. Blanksby, C. Barner-Kowollik, J. Cornil and P. Gerbaux, *J. Am. Soc. Mass Spectrom.*, 2024, **35**, 2408–2419.

69 Q. Duez, F. Chirot, R. Liénard, T. Josse, C. Choi, O. Coulembier, P. Dugourd, J. Cornil, P. Gerbaux and J. De Winter, *J. Am. Soc. Mass Spectrom.*, 2017, **28**, 2483–2491.

70 V. Gabelica, A. A. Shvartsburg, C. Afonso, P. Barran, J. L. P. Benesch, C. Bleiholder, M. T. Bowers, A. Bilbao, M. F. Bush, J. L. Campbell, I. D. G. Campuzano, T. Causon, B. H. Clowers, C. S. Creaser, E. De Pauw, J. Far, F. Fernandez-Lima, J. C. Fjeldsted, K. Giles, M. Groessl, C. J. Hogan, S. Hann, H. I. Kim, R. T. Kurulugama, J. C. May, J. A. McLean, K. Pagel, K. Richardson, M. E. Ridgeway, F. Rosu, F. Sobott, K. Thalassinos, S. J. Valentine and T. Wyttenbach, *Mass Spectrom. Rev.*, 2019, **38**, 291–320.

71 BIOVA - San Diego: Dassault Systèmes, Materials Studio, 2022.

72 J. Gasteiger and M. Marsili, *Tetrahedron Lett.*, 1978, **19**, 3181–3184.

73 M. F. Mesleh, J. M. Hunter, A. A. Shvartsburg, G. C. Schatz and M. F. Jarrold, *J. Phys. Chem.*, 1996, **100**, 16082–16086.

74 S. A. Ewing, M. T. Donor, J. W. Wilson and J. S. Prell, *J. Am. Soc. Mass Spectrom.*, 2017, **28**, 587–596.

75 M. J. Frisch, G. W. Trucks, H. B. Schlegel, G. E. Scuseria, M. A. Robb, J. R. Cheeseman, G. Scalmani, V. Barone, B. Mennucci and G. A. Petersson, *Gaussian2009*, 2009.

76 T. Steiner, *Angew. Chem., Int. Ed.*, 2002, **41**, 48–76.

77 A. Boehmke Amoruso, R. A. Boto, E. Elliot, B. De Nijs, R. Esteban, T. Földes, F. Aguilar-Galindo, E. Rosta, J. Aizpurua and J. J. Baumberg, *Nat. Commun.*, 2024, **15**, 6733.

78 S. Grimme, J. Antony, S. Ehrlich and H. Krieg, *J. Chem. Phys.*, 2010, **132**, 154104.

79 Ł. M. Mentel and E. J. Baerends, *J. Chem. Theory Comput.*, 2014, **10**, 252–267.